INTERFACE SCIENCE, 2, 425–440 (1995)

Off-Axis Electron Holography of Hetero-Interfaces

M. GAJDARDZISKA-JOSIFOVSKA mgj@csd.uwm.edu
Department of Physics and Laboratory for Surface Studies, University of Wisconsin Milwaukee, P.O. Box 413, Milwaukee, WI 53201

Abstract. Off-axis electron holography is one of the new emerging methods for high spatial resolution characterization of interfaces in materials. It enables recording and retrieval of both amplitude and phase of an electron wavefunction scattered by a specimen. Phase changes introduced by magnetic and electrostatic fields have been studied in the first applications of electron holography to domain walls in ferromagnetic and ferroelectric materials and to *p-n* junctions. Planar defects in single crystals, such as stacking faults, have been observed with strong phase contrast due to dynamical diffraction.

Applications to heterogeneous interfaces have only started. High phase contrast due to mean inner potential differences is found for interfaces between high and low atomic number materials. Dynamical contributions to the phase of the transmitted beam are important for epitaxial interfaces in strongly diffracting orientations. Numerical hologram reconstructions yield quantitative amplitude and phase images of an interface which are energy filtered and are in perfect registry. Both are function of specimen thickness. The thickness dependence can be eliminated by division of the phase image with a logarithm of the amplitude image. This ratio maps the product of the mean inner potential and the mean free path for inelastic scattering across a hetero-interface in weekly diffracting orientations.

Resolution enhancement through aberration correction has not been demonstrated for interfaces as yet. Holography of interfaces in plan view is unexplored.

Keywords: electron holography, interface microscopy techniques, energy filtering, Mo/Si multilayers

1 Introduction

When an electron is scattered by an object both its amplitude (A) and phase (φ) are altered. But when the scattered wave is recorded, only its amplitude is detected in the intensity image ($I = \psi\psi^* = Ae^{i\varphi}Ae^{-i\varphi} = A^2$). Holography was invented by Gabor [1] as method of preserving both amplitude and phase information in an electron intensity image. The preservation of phase information is important in electron microscopy because most samples are phase objects, i.e. they introduce phase changes. In addition, the aberrations of the electron optics also cause phase changes which limit the resolution of the microscope. Gabor originally proposed holography as a method for enhancing the resolution of electron microscopes. The concept applies to any wave-optics experiment performed with coherent sources, as witnessed by the many applications of holography in laser optics.

Holography, in the most general sense, is any method which allows recording and retrieval of both the amplitude and phase of a wave scattered by an object. A two step process is used, consisting of recording and reconstruction. In the recording step, an interference pattern is formed by overlapping the wave scattered by the object with a coherent reference wave. The selection of the reference wave distinguishes between the different forms of holography. The first discrimination is between in-line and off-axis holography, as reviewed for electrons by Tonomura [2]. The further details of the experimental setup allow to name more than twenty forms of electron holography, as described recently by Cowley [3]. The reconstruction step is specific to each holography method.

For the case of solid interfaces, off-axis electron holography appears to be the most promising method, and is the only one that has been used in the relatively limited number of studies [4]. The basic setup for off-axis electron holography in a transmission electron microscope is illustrated in Fig. 1. There are two major differences between this experiment and conventional transmission electron microscopy: Firstly, the illumination has to be coherent for holography, and secondly a biprism is needed to form an off-axis hologram. Details of the experimental requirements are presented in section 2.

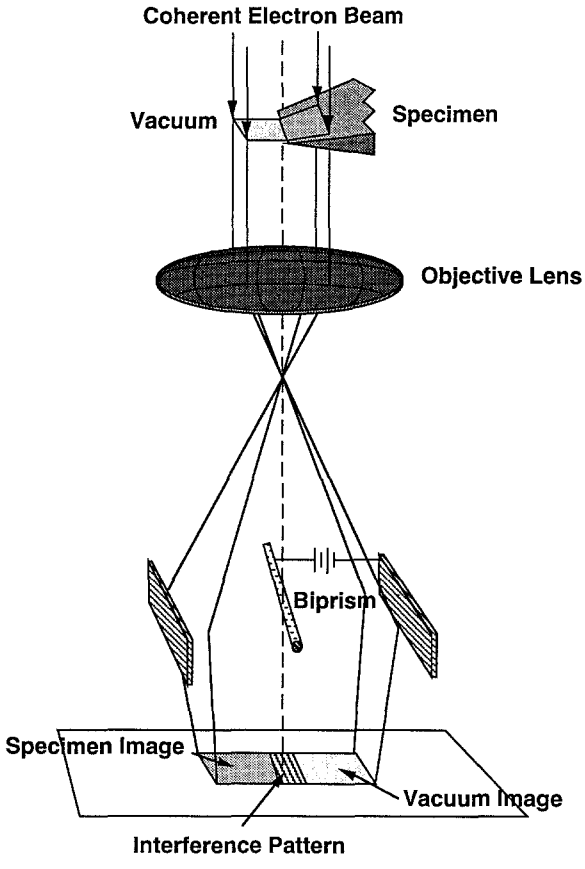

Fig. 1. Schematic diagram of the experimental setup used for off-axis transmission electron holography. (Courtesy of J.K. Weiss)

The ray diagram in Fig. 1 illustrates the simplest mode of off-axis holography when an electron transparent specimen is illuminated such that a portion of the wavefront passes through vacuum only. The latter serves as a reference wave. The wave transmitted through the specimen carries the information about this object in its amplitude and phase. After passing through the microscope objective lens, the object and reference wavefronts are tilted towards each other by a positively charged electron biprism. An interference pattern forms in the region of overlap. This pattern is the off-axis hologram. It is further magnified by the projector lenses of the microscope and recorded as an intensity image. The amplitude information is encoded in the intensity of the holographic interference fringes, while the phase information is encoded in the position of the interference fringes. This information is separated in the hologram reconstruction process. The basic theory of the hologram reconstruction is reviewed in section 3, along with some practical aspects pertaining to interface studies.

With the advent of digital hologram recording and numerical reconstructions, holography has become an accurate quantitative method. The reconstructed phase image is the grand prize of holography. However, we have recently realized that much is to be gained by combining the amplitude and phase information from the same hologram. Section 4 summarizes the present understanding of hologram interpretation, and reviews the applications of off-axis holography to studies of homogeneous and heterogeneous interfaces. The advantages and limitations of the method are discussed. Results from our studies of hetero-interfaces are used as illustrations throughout this paper.

2 Experimental Requirements

2.1 Instrumentation

A coherent electron source and an electron biprism are the basic requirements for experimental off-axis holography. A field emission gun (FEG) provides illumination with the needed temporal and spatial coherence [2]. The temporal coherence is limited by the energy spread of the electrons. The spatial coherence is achieved by spreading of the illumination to obtain a plane incident wavefront over the field of the hologram. The brightness of the source limits the attainable spatial coherence. Astigmatic illumination, as proposed originally by Lauer [5], enables improvement of the spatial coherence in off-axis electron holography (e.g. see Hanszen's description for advantages of astigmatic illumination [6]).

The off-axis hologram is formed with use of an electrostatic biprism of the Möllenstedt-Düker type [7]. In the most standard setting, the biprism is a positively biased wire, mounted on an insulating post, and placed in the image plane of the objective lens. The objective and the first intermediate lens currents are changed from the normal TEM operation in order to move the image plane below the biprism, thus providing imaging of the hologram. It should be noted that the biprism can also be biased negatively and placed at other positions in the microscope column, followed by appropriate lens settings (e.g. [8]).

The hologram is recorded as any other electron intensity image or diffraction pattern. Photographic emulsion has been used for most of the published data with subsequent optical reconstruction of the hologram (e.g. [2] and references therein). Digitization of the photographic image has enabled numerical reconstruction of

holograms (e.g. [9]). Slow-scan CCD cameras are now becoming the detector of choice for holography [10] because of their linear response, and the digital form of the data which enables direct application of numerical hologram reconstruction procedures (section 2.3).

The experimental holography results in this work were obtained with the Arizona State University's Philips EM400ST-FEG transmission electron microscope operated at 100 keV: i) The electron source was a thermally assisted tungsten field emission gun; ii) A non-rotatable biprism was used in the selected area aperture position; iii) Astigmatic illumination was used with ≈10:1 ratio between the directions perpendicular and parallel to the biprism; iv) A Gatan 679 slow-scan CCD camera was used to record 1024 × 1024 px digital holograms with typical exposure times of 1s.

2.2 *Interface and Biprism Orientation*

The specimen geometry, and its orientation with respect to the biprism wire, are the most important choices in an interface holography experiment. It may therefore be timely to discuss the different possibilities and compare their advantages and shortfalls. All of the existing holography studies of solid interfaces have used an edge-on orientation of the interface with respect to the incident electron direction. This orientation provides the best spatial resolution. Figure 2 illustrates four basic orientations for edge-on interface holography. The position of the hole in the specimen is important for cases when vacuum is used as an absolute reference for the phase (Fig. 2a and b). The orientation in (a), where the biprism is parallel to the interface, is most favorable for studies of ion-milled cross-sectional specimen of films grown on a substrate [11–14]. Shaded lines are drawn at the bottom of Fig. 2a to illustrate the position of the holographic fringes. The spacing between the fringes is altered by different amounts in the materials *A* and *B* which form the interface. This specimen-biprism geometry is favorable for holographic reconstruction (as described in the following section), but is unsuitable for interferometric measurements. The latter are direct phase measurements from the hologram, obtained by tracing one holographic fringe and measuring it's departure from a straight line. This shift is then converted to radians using the 2π distance between two neighboring fringes as a calibration (see example in Fig. 3 showing holographic fringe shifts across a $CoSi_2$/Si interface; this interface is positioned at an angle to the biprism, an orientation which will be discussed at the

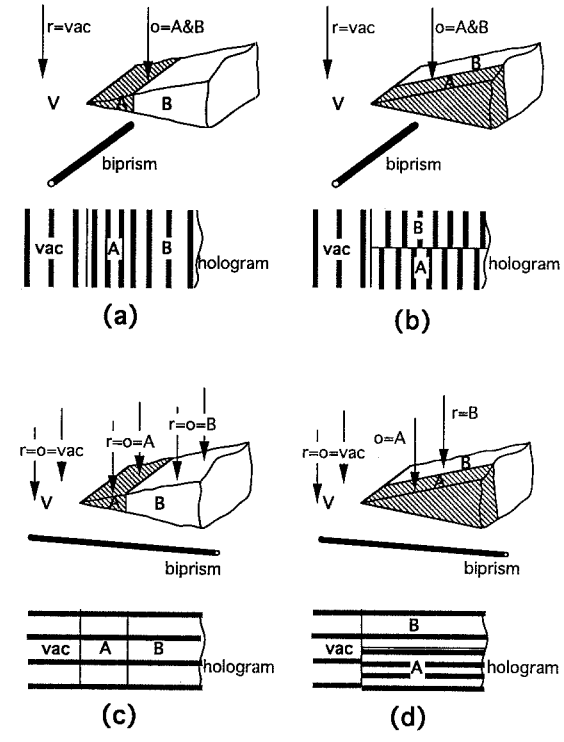

Fig. 2. Schematic representation of the four basic orientations of the interface (*i*) with respect to the biprism (*b*) and the resulting shifts of holographic fringes: (a) $i \parallel b$, reference wave (*r*) in vacuum; (b) $i \perp b$, reference wave in vacuum; (c) $i \perp b$, reference and object wave (*o*) in same medium, (d) $i \parallel b$, reference wave in one of materials forming the interface.

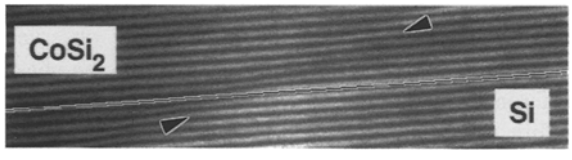

Fig. 3. Hologram from interface (arrowed) between Si substrate and epitaxial $CoSi_2$ film. Shift of holographic fringes across interface is visible and directly measurable. Line extrapolates one dark fringe from Si into $CoSi_2$ to illustrate fringe shift.

end of this section). Since departures from straightness of a line are easier to measure than changes in spacing between lines, the orientation in Fig. 2a should be avoided if quick, but less accurate, phase measurements are needed directly from the hologram.

The orientation in Fig. 2b is suitable for both direct interferometric measurements and for holographic reconstruction. This interface geometry is typical for cleaved wedges of epitaxial films [15], but is found only by chance in ion milled samples of thin films. This

orientation is also best for studies of grain boundaries in polycrystalline samples [12, 16]. Vacuum is used as a reference and the measured phase is absolute. The phase becomes relative when there are electric fields in the specimen, as in the case of a biased *p-n* junction. In this instance it was shown that leakage fields extend over microns into vacuum, and the reference wave is not a simple plane wave any more [17–19].

Relative phases are sometimes desirable, but more often the orientations illustrated in Fig. 2c and d are used in instances when the interface of interest is far from a hole in the specimen, thus preventing the use of vacuum as a reference. The orientation in (c), with the biprism perpendicular to both the interface and the edge of the specimen, has a most complicated reference wave which changes in the direction of the biprism wire: It is vacuum first, material *A* in the middle and material *B* at the end, with the object wave also changing in the same order. When the biprism is exactly perpendicular to the interface, *and* the specimen thickness and composition does not vary in the direction parallel to the interface, there should be no phase changes and therefore no fringe shifts across the interface. This situation has been first demonstrated by Miyake et al. [20] on an equivalent case of a chrysotile fiber: They observed disappearance of the fringe shift at the vacuum/fiber interface when the fiber was positioned as in Fig. 2c. In such instances the orientation in Fig. 2c is useless, or rather it can be used to check that there are no inhomogeneities in the specimen thickness and composition along the interface direction.

When the holographic fringe shifts are observed across an interface positioned as in Fig. 1c, the phase difference between the reference and object wave within the same material (vac-vac, *A-A* and *B-B*) can be caused by: magnetic fields, electric fields [21] and/or diffraction effects [22] in the specimen producing beam tilts perpendicular to the biprism wire. A large shift of the whole interference pattern across the interface was observed [22] for the orientation (c) when the thickness of the specimen matches an extinction distance in one of the two materials. In this special case, the object and reference wave in that material are given by the diffracted wave, which is tilted by a Bragg angle perpendicular to the biprism wire.

Finally, the orientation in Fig. 2d uses only one of the materials (i.e. the substrate *B*) as a reference wave and yields the relative phase change (i.e. the difference in phase between *A* and *B*). It should be remembered that even if a vacuum region is included in the hologram, the phase measurements are not absolute. This orientation is suitable for reconstructions, and should be used in cases when only the relative phase is desired, or vacuum is not available for a reference (an example of such reconstructed hologram will be given in Fig. 9).

When the biprism is not rotatable, the interface is likely to be at an angle other than the 0° or 90° which were illustrated in Fig. 2. For example Fig. 3 shows part of a hologram in which the $CoSi_2$/Si interface is at ≈35° with respect to the biprism. Vacuum was used as a reference in this hologram, and this situation is a combination of Fig. 2a and b. The phase change measured is absolute, and because of the visible shift of the fringes across the interface (as in Fig. 2b) direct interferometric measurements are possible from the hologram. However such measurements of the phase are meaningful only for uniform interfaces and constant specimen thickness when the measured phase shift is the same across any point on the interface. Therefore, for most of the interface studies it is best to obtain the phase (and amplitude) measurements after reconstruction of the hologram.

3 Hologram Reconstruction

The principles of off-axis hologram reconstruction have been described in many original and review articles (e.g. see Tonomura's [2] and Lichte's [9] recent reviews). Recently we have discussed the case of numerical reconstructions of digital holograms from hetero-interfaces [12, 13, 23]. For sake of completeness, this paper will review the basic concepts, and illustrate them with new experimental results from interfaces.

3.1 Theoretical Background

The intensity in an off-axis hologram can be written as [23]:

$$I_{\mathrm{hol}}(\mathbf{r}) = \left\{A_r^2 + A_o^2(\mathbf{r}) + 2A_r A_o(\mathbf{r}) \cos[4\pi \Delta\mathbf{K} \cdot \mathbf{r} + \phi_r - \phi_o(\mathbf{r})]\right\} + A_i^2(\mathbf{r}) \quad (1)$$

The cosine term in this equation represents the holographic fringes with spatial period $(2\Delta\mathbf{K})^{-1}$ which is modified by the phase difference between the reference and the object waves: $\Delta\phi = \phi_r - \phi_o(\mathbf{r})$. When both the reference and object wave pass through vacuum the fringe spacing is constant and is determined only by the beam tilt due to the biprism ($\pm\Delta\mathbf{K}$). The intensity of

the holographic fringes is $2A_rA_o$ where A_r is the amplitude of the reference wave and A_o is the amplitude of the object wave. The fringes are superimposed on a background with intensity $A_r^2 + A_o^2(\mathbf{r}) + A_i^2(\mathbf{r})$, where A_i^2 is intensity due to incoherence of the illumination and inelastic scattering in the material [13, 24]. The reference and object waves in Eq. 1 also carry information about the point spread function of the objective lens $G(x, y)$ through which the two waves pass before being superimposed by the biprism. Therefore, A_o and ϕ_o in Eq. 1 describe the amplitude and phase of the object image wave which are connected with the amplitude a_o and the phase φ_o of the object exit wave through a convolution with G (e.g. [25]):

$$A_o(x, y)\exp[i\phi_o(x, y)] = \{a_o(x, y)\exp[i\varphi_o(x, y)]\} \otimes G(x, y) \quad (2)$$

The same equation holds for the reference wave.

The use of tilted waves is the main advantage of off-axis holography. It enables separation of the background intensity in the central (autocorrelation) part of the Fourier transform of the hologram, but more importantly it separates the two conjugate images in the two sidebands centered at $+2\Delta\mathbf{K}$ and $-2\Delta\mathbf{K}$ respectively:

$$\begin{aligned}\mathrm{FT}[I_{\mathrm{hol}}(\mathbf{r})] &= \delta(\mathbf{u}) \otimes \mathrm{FT}\left[A_i^2 + A_r^2 + A_o^2(\mathbf{r})\right] \quad \text{(autocorrelation)} \\ &+ \delta(\mathbf{u} + 2\Delta\mathbf{K}) \otimes \mathrm{FT}\{A_rA_o(\mathbf{r})\exp[i(\phi_r - \phi_o(\mathbf{r}))]\} \quad \text{(sideband)} \\ &+ \delta(\mathbf{u} - 2\Delta\mathbf{K}) \otimes \mathrm{FT}\{A_rA_o(\mathbf{r})\exp[-i(\phi_r - \phi_o(\mathbf{r}))]\} \quad \text{(sideband)} \end{aligned} \quad (3)$$

The Fourier transformation of the hologram can be performed numerically (as was done for all the reconstructed images in this paper and discussed in section 3.2) or optically (by illuminating the electron hologram with a parallel laser beam and observing the optical diffractogram at the back focal plane of a convex lens [2, 6]). In both numerical and optical reconstructions only one of the sidebands is selected using a numerical or a physical aperture respectively. In the numerical reconstruction the sideband is extracted and inverse Fourier transformed to give the complex reconstructed image:

$$\begin{aligned} I_{\mathrm{rec}}(\mathbf{r}) &= \mathrm{FT}^{-1}\mathrm{FT}\{A_rA_o(\mathbf{r})\exp[i(\phi_r - \phi_o(\mathbf{r}))]\} \\ &= A_rA_o(\mathbf{r})\cos[\phi_r - \phi_o(\mathbf{r})] + iA_rA_o(\mathbf{r}) \\ &\quad \times \sin[\phi_r - \phi_o(\mathbf{r})] = \mathrm{Re} + i\ \mathrm{Im} \end{aligned} \quad (4)$$

The phase image is calculated from this complex image as $\phi_r - \phi_o(\mathbf{r}) = \tan^{-1}(\mathrm{Im}/\mathrm{Re})$. It maps the spatial variations in the phase of the object wave with respect to the phase of the reference wave. The retrieval of this phase of the image wave is impossible without holography.

The modulus of the complex image is $\sqrt{\mathrm{Re}^2 + \mathrm{Im}^2} = A_rA_o(\mathbf{r})$. It is usually called amplitude image, a term which is correct when the reference wave goes through vacuum and provides only a constant gain A_r for the object amplitude $A_o(\mathbf{r})$.

It is very important to note that both the amplitude and phase images are energy filtered [13, 24, 26, 27], as the inelastic scattering contributions A_i are incoherent and do not contribute to the sidebands in Eq. 3.

3.2 *Practical Aspects of Numerical Hologram Reconstruction*

The size of the selected sideband is important because it defines the resolution in the reconstructed image [25]. Figure 4 illustrates this point using a hologram from GaAs/$Ga_{0.7}Al_{0.3}As$ triangular quantum well. The specimen orientation with respect to the biprism was close to that in Fig. 1b. The top raw in Fig. 4 shows the logarithm of the modulus of a 256×256 pixel sideband extracted from a 1024×1024 pixel FFT of a hologram. The square sideband is further restricted by superposition of a circular aperture with a 5 pixel wide soft edge (note that a circular aperture is not required for a holographic reconstruction; a square sideband can be used directly). Four different radii are used for the aperture: 2 nm^{-1}, 1 nm^{-1}, 0.67 nm^{-1} and 0.5 nm^{-1}, corresponding to resolution in the reconstructed amplitude and phase images of: 0.5 nm, 1 nm, 1.5 nm and 2 nm. The Fresnel fringes from the biprism edges, which show particularly well in the top right corner of the reconstructed images, can be used to spot quickly that the resolution in the images decreases as smaller apertures are imposed on the sideband. In the images with 2 nm resolution (right side of tableau) only the first three bright Fresnel fringes are visible, while the visible fringes cover the whole field of view in the 0.5 nm resolution amplitude and phase images.

The amplitude and phase images are quantitative and they are in perfect registry with each other. Therefore it is often useful to extract image profiles for quantitative comparison and analysis. The profiles shown in Fig. 4 give the values of the amplitude and the phase in the central 1 pixel-wide-column (profiles in left column), and from the central 1 px-wide-row (profiles in right

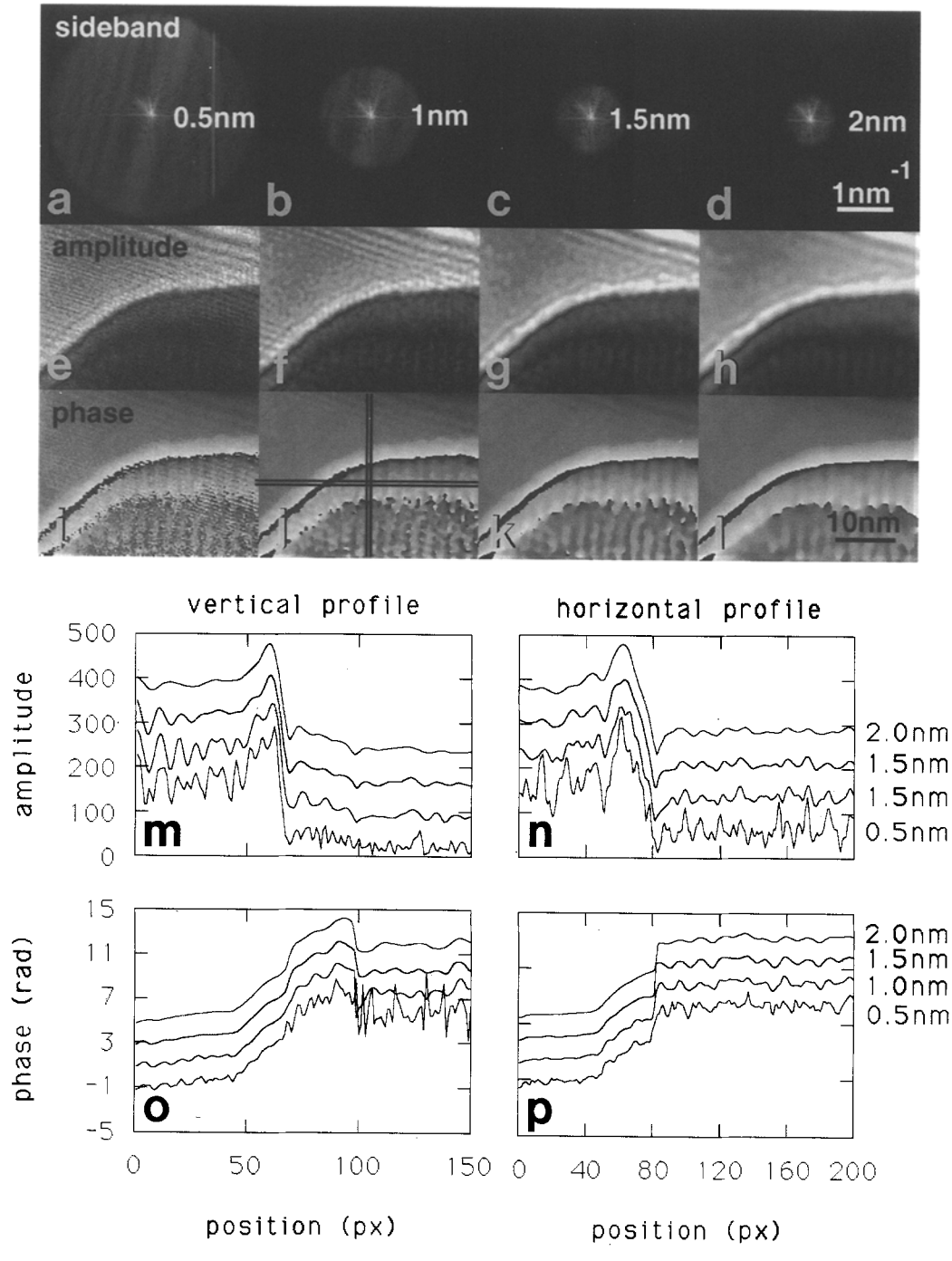

Fig. 4. Reduction of sideband aperture size (a–d) results in decreased resolution in reconstructed amplitude (e–h) and phase (i–l) images: i.e. sideband (a) gives amplitude (e) and phase (i) images with 0.5 nm resolution. Profiles extracted from amplitude (m, n) and phase (o, p) images show values of central pixel column (vertical profiles m and o) and the central pixel row (horizontal profiles n and p) for reconstructed images with decreasing resolution. Position of extracted raw and column are indicated with lines in phase image (j).

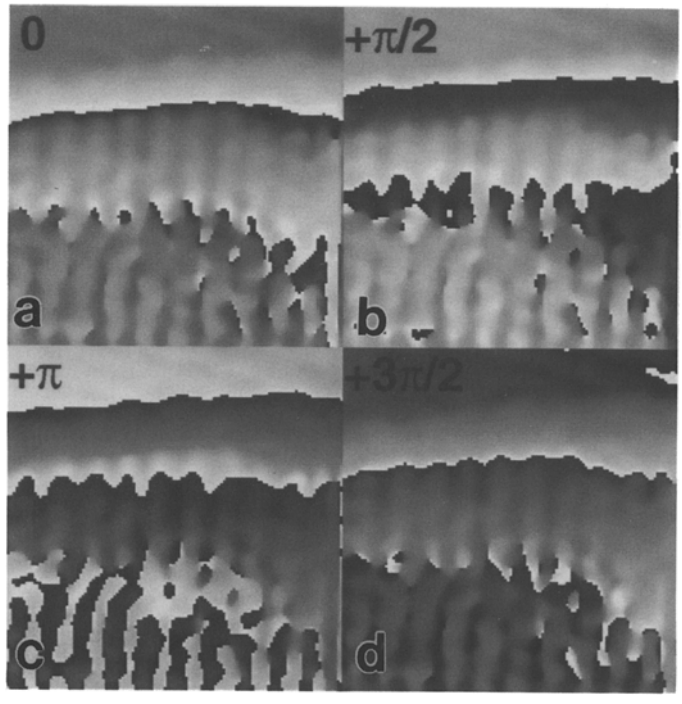

Fig. 5. Shifting of position of wrapping in reconstructed phase image of GaAs/$Ga_{0.7}Al_{0.3}As$ triangular quantum well. Reconstructed complex image (see Eq. 4) has been multiplied by: a) 1; b) i; c) -1 and d) $-i$, before calculating these phase images.

column). The profiles from images with different sideband apertures are displayed with equidistant offsets, and the phase profiles are numerically unwrapped (as will be discussed shortly). We want to draw the attention to the smoother profiles obtained from the images with poorer resolution. The smaller aperture in the sideband acts as an averaging filter, thereby reducing the noise in the reconstructed image and the extracted profile, at the expense of a poorer image resolution. It is also important to note that the reduced size of the sideband aperture does not change the shape of the profiles, apart from the smoothing. Thus, the positions of the abrupt minima at the extinction thicknesses in the amplitude image, and the corresponding positions of the phase jumps due to double diffraction, are unaltered by the aperture size. Slopes measured from phase images are also independent of the size of the sideband aperture as long as the sideband is well separated from the autocorrelation [28]. For atomic resolution holography the sideband should have a radius smaller or equal to 1/3 of the separation between the autocorrelation and the sideband centers [25]. This corresponds to resolution in the reconstructed image of 3 times the holographic fringe spacing. For lighter materials, and for crystals oriented in weekly diffracting conditions the size of the sideband can be $\approx 1/2$ of the holographic fringe frequency in vacuum [29].

The phase image calculation is subject to "phase wrapping" which results from the limited range of the principal arctangent function used to calculate the phase. Discontinuous phase jumps from π to $-\pi$ are observed when the phase in the complex image changes by more than 2π. The phase wrapping can be removed by numerical phase unwrapping algorithms, or by shifting of the phase image by a desired phase angle α. The latter is achieved by multiplying the complex image from Eq. 4 with a complex constant: $\cos\alpha + i\sin\alpha$. The angle α can be selected by trial and error to remove the phase wrap from a region of interest in the image [28]. A more systematic procedure involves the shifting of the complex image in intervals corresponding to $\pi/2$ (i.e. complex constants: i, -1, $-i$) [12]. This is illustrated in Fig. 5 for the GaAs/$Ga_{0.7}Al_{0.3}As$ sample of Fig. 4k. The different wrap-free regions of the tableau can now be cut and pasted into a complete unwrapped image, after shifting them back by the real constant $n\pi/2$. The tuning of the phase wrapping can also be useful for enhancement of the phase contrast at

interfaces between similar materials (e.g. bottom half of Fig. 5c).

After the unwrapping, the phase image can also be corrected for geometrical distortions introduced by the projector lenses and the detector. This correction is carried by subtracting a phase image of vacuum from the phase image of the specimen. The vacuum image is reconstructed from a "flat field" hologram recorded by removing the specimen without altering the other experimental conditions [10]. Finally this resultant image can be corrected for tilts introduced by the inaccuracies in the selection of the sideband center: A plane is fitted to a region of the phase image containing vacuum only (specimen condition as in Fig. 2a and b). This calculated plane is then subtracted from the phase image resulting in a flat vacuum with zero phase (e.g. [28]). The absolute phase is now directly readable at any point in the phase image and quantitative phase profiles can be extracted without any further adjustments. All of the above corrections have been performed on the reconstructed images shown in this paper.

4 Interpretation of Interface Holograms

The field of hetero-interface holography is very young [11], and much work is needed to accumulate experimental results and to develop methods for their quantitative interpretation. Here we will review the present state of knowledge.

A starting point for the understanding of the phase image can be provided by the general expression [30]:

$$\phi(\mathbf{r}) = -\frac{2\pi e}{\lambda E}\frac{E_0 + E}{2E_0 + E}\int_l V(\mathbf{r})ds - \frac{2\pi e}{h}\int_l \mathbf{A}(\mathbf{r})\cdot d\mathbf{s} \tag{5}$$

which shows that the phase of an electron wave is altered by all electrostatic (scalar: V) and magnetic (vector: $\mathbf{A}$) potentials along the electron trajectory (l). The constants in Eq. 5 have their usual meaning (e—electron charge, λ—electron wavelength, E_0—electron rest energy, E—electron energy and h—Plank's constant). The phase changes introduced by the magnetic field of the objective lens can be expressed using the transfer function theory (as in Eq. 2). In this case the integration in Eq. 5 can be performed only over the thickness of the specimen in the electron beam direction (t). The last term is then consequential only for magnetic materials, as demonstrated in the many important experiments by the Tonomura group: Electron holography has been used to study fields in magnetic particles, across domain walls in ferroelectrics, and penetrating through superconductors as fluxons (see [2] and references therein). However, hetero-interfaces in magnetic materials have not been investigated as yet.

The scalar potential term in Eq. 5 contributes to every hologram through the specimen atomic potentials. This term also represents additional electrostatic fields in the material. The latter contribution has been studied in holograms from *p-n* junctions [17, 18], ferroelectric domain walls [21] and grain boundaries in electroceramics [22], but no results have been reported for electrostatic fields at hetero-interfaces.

In the following discussion we will distinguish between high resolution and moderate resolution holography of interfaces. The former is concerned with atomic potentials in specimen orientations when the projected potential is periodic. The latter is concerned with the average atomic potential (i.e. the mean inner potential), with phase and amplitude changes due to dynamical scattering, and with electrostatic and magnetic fields which change over distances much larger than the interatomic spacing.

4.1 High Resolution Holography

The coherent illumination enables improved instrumental resolution, while electron holography enables enhancement of the point resolution through deconvolution of the point spread function. Much of the current research in electron holography is directed towards optimization of hologram recording and reconstruction methods for ≈0.1 nm resolution. Known perfect crystals are being used as tests [31, 32]. No exit-wave restoration has been reported for interfaces at this time.

The complete understanding of the perfect crystal case is needed before holography could be applied to enhanced atomic resolution imaging of interfaces. It can be expected that the full aberration correction will be more involved for holograms of interfaces. Much development is needed in this field, but some of the important rewards for studies of interface structures may be predicted: The superior point resolution of aberration corrected images should enable better initial models of the interface structure, which could then be improved via the established image simulation methods. The comparison of simulated and experimental images should also become more reliable by having an amplitude and a phase image to match against. In addition, the sideband of the hologram is a numerical diffractogram which is sensitive to the crystal tilt [33]. This allows a posteriori "nanodiffraction" from

any chosen part of the holographic image which should significantly reduce the range of crystal tilts used for simulation of the exit wavefunction.

4.2 *Moderate Resolution Holography*

When the phase image is needed to map changes in mean inner potential, or variations in electric and magnetic fields across interfaces, the length scales are typically much larger than the resolution of the used electron microscope. In these cases it is most favorable to record the holograms at Gabor defocus, which can be expressed in terms of the spherical aberration coefficient C_s and the wavelength of the electrons (λ) as:

$$\Delta f_{\text{Gabor}} = -0.68\sqrt{C_s\lambda} \tag{6}$$

At the Gabor defocus, the objective lens transfers the widest band of spatial frequencies of the object wave to the image wave without alterations of its phase and amplitude [34]. This is contrary to the Scherzer defocus ($\Delta f_{\text{Scherzer}} = -1.2\sqrt{C_s\lambda}$), optimal for high resolution electron microscopy, at which the phase of the object wave is transferred into the amplitude of the image wave.

Gauss defocus ($\Delta f_{\text{Gauss}} = -0.3\sqrt{C_s\lambda}$) is a good practical alternative for Gabor defocus in moderate resolution holography. In both cases, the phase of the object wave is transferred into phase of the image wave. The Gauss defocus is easier to set: one looks for a minimum contrast image. This convenience results in small reduction of the directly interpretable image resolution. For example, for the lens used in this work, the resolution at Gabor defocus is ≈0.5 nm, while at Gauss defocus it is ≈0.7 nm. Most of the holograms in this paper were recorded at Gaussian defocus. Under these conditions the restoration of the exit wave is not necessary. Therefore, in moderate and low spatial resolution electron holography one can speak of phase and amplitude images without any further specification.

In absence of electric and magnetic fields, the volume average of the atomic potentials, i.e. the mean inner potential V_0, determines the phase change in the kinematical diffraction limit:

$$\phi = -\frac{2\pi e}{\lambda E}\frac{E_0 + E}{2E_0 + E}V_0 t \tag{5a}$$

The mean inner potential contribution to the phase image is always present and needs to be accounted for in quantitative phase measurements. The following discussion will consider interfaces between materials

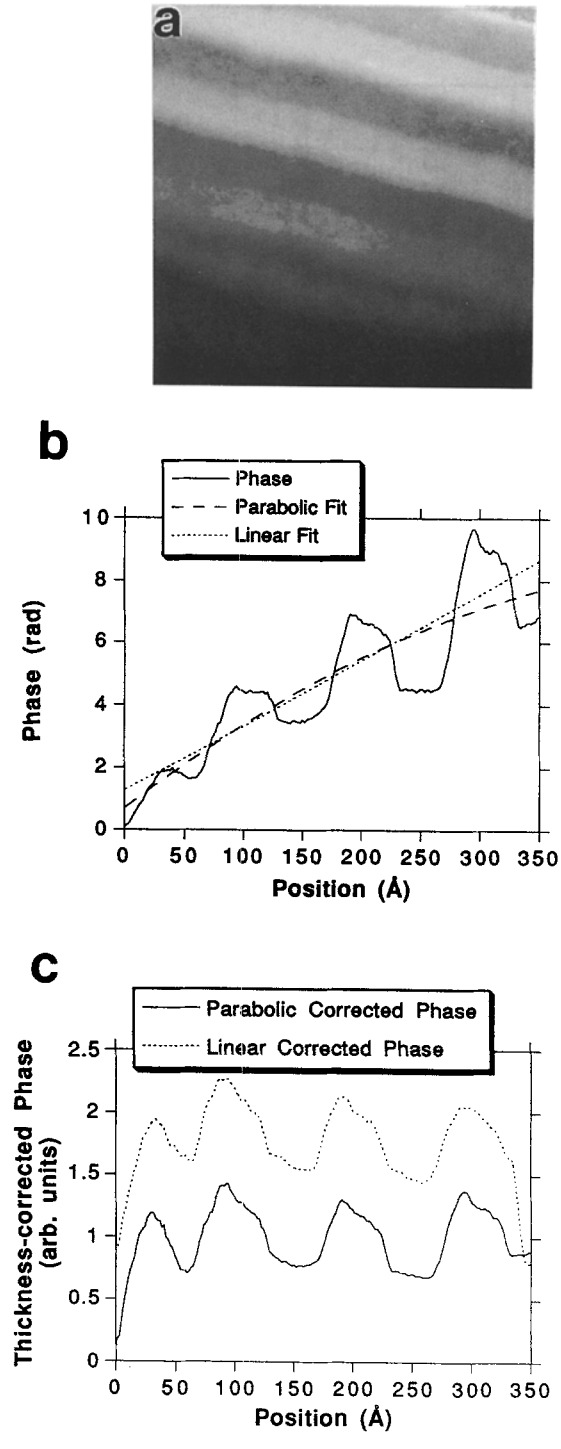

Fig. 6. First hologram from hetero-interface: (a) Reconstructed phase image of Mo/Si multilayer; (b) Phase profile with two model thickness profiles; (c) Thickness corrected phase profile. (Courtesy of J.K. Weiss)

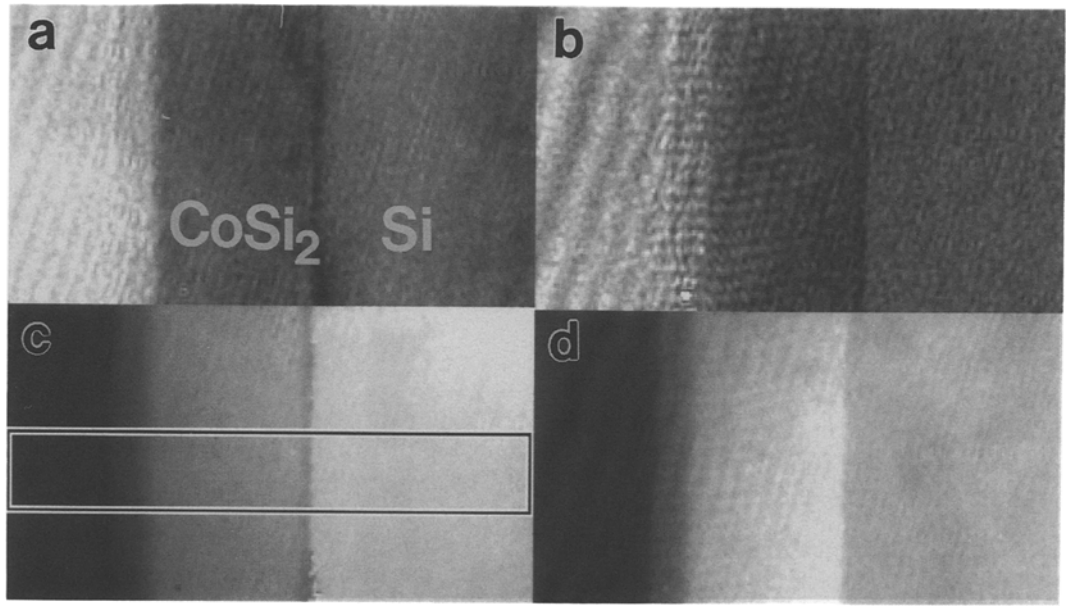

Fig. 7. Amplitude (a, b) and phase (c, d) images reconstructed from two holograms of $CoSi_2$/Si interface oriented with [011] zone parallel to the beam (a, c) and in (200) systematic row orientation (b, d). Note contrast reversal in phase image upon tilting. Box with length of 30 nm marks region used for profiles shown in [23].

with different crystallinity and differences in mean inner potential.

4.2.1 Interfaces in Amorphous and Polycrystalline Materials: Effects of Mean Inner Potential and Specimen Thickness. The first published phase image of a hetero-interface is shown in Fig. 6a [11]. The sample is a multilayer of amorphous Si and polycrystalline Mo with a large difference in mean inner potential between the two kinds of layers ($\Delta V_0 = (8 \pm 2)V$ as measured from interface refraction effects in nanodiffraction [35]). The phase profile in Fig. 6b shows that, in addition to the thickness dependence, the phase advances more in the Mo layers compared to the Si layers. The asymmetrical width of the Mo/Si and Si/Mo interfaces confirms previous HREM observations about these multilayers [36]. Subtraction of a parabolic fitted profile in Fig. 6c removes the thickness dependence. The obtained profile maps the change of the mean inner potential across the interfaces, as in Eq. 5a, albeit in arbitrary units. The mean inner potential depends on the composition and the structure of the material. In general, materials with higher density have larger mean inner potential (i.e. larger $|V_0|$, since V_0 is negative). Therefore, materials with densely packed light atoms may have similar mean inner potential as materials with higher atomic numbers and larger interatomic distances. Weiss et al. [12] have demonstrated such lack of phase contrast in holograms from hetero-interfaces between amorphous Si and SiN_x.

4.2.2 Crystal Interfaces: Effects of Crystal Tilt. The tilt of the specimen is very important for holography from crystals. We have shown recently that, when the crystals are tilted to weekly diffracting conditions, the kinematical approximation for the phase is valid to accuracy of better than 5%, even for crystal thickness of ~100 nm [28]. However, for epitaxial interfaces, the tilt options are usually restricted to zone axis and systematic row orientations for edge-on viewing of the interface. For Si crystals tilted to a {220} systematic row we have shown that the dynamical contributions are ~10% of the V_0 contributions to the phase, but for samples tilted to zone axis the dynamical contributions become substantial [28].

Figure 7 demonstrates the effects of tilt on holograms from a $CoSi_2$/Si(100) interface grown by molecular beam epitaxy [15, 23]. This system is an example of crystal/crystal interface with large change in mean inner potential ($\Delta V_0 = 9.1$ V was calculated using a non-binding approximation [17]). The amplitude im-

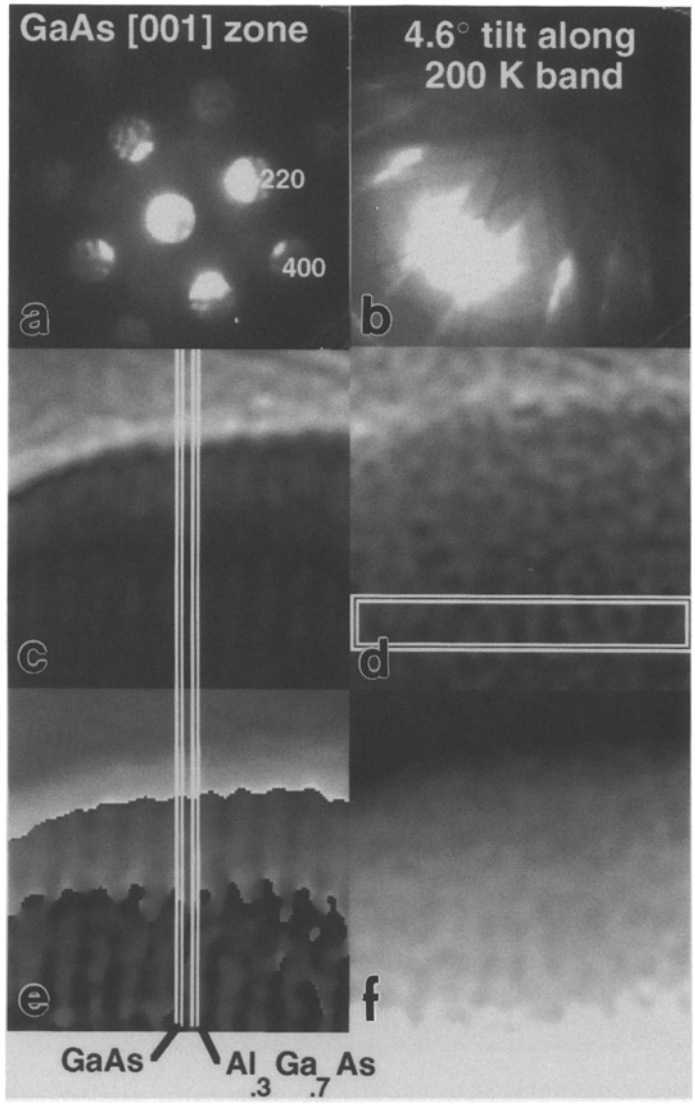

Fig. 8. Tilting from zone axis (a, c, e) to systematic row (b, d, f) orientation causes loss of amplitude (c, d) and phase (e, f) contrast for GaAs/$Al_{0.3}Ga_{0.7}As$ quantum well structure. Reconstructed hologram images are 23 nm wide. (Box and lines mark positions for profiles not shown here.)

ages (top) show similar contrast in the [110] zone axis (Fig. 7a) and the systematic (002) row (Fig. 7b) orientation, but the contrast between the phase in $CoSi_2$ and Si inverts due to the tilting (Fig. 7c and d). When the incident beam is parallel to the {002} crystal planes (*d*), the phase advances more in $CoSi_2$ compared to Si which is qualitatively consistent with $CoSi_2$ having larger mean inner potential than Si. When the transmitted beam is parallel to the [110] zone (*c*), the dynamical contributions are stronger, causing reversal of the phase contrast from that which is expected from the V_0 dependence solely.

The same tilting experiment is shown in Fig. 8 for GaAs/$Al_{0.3}Ga_{0.7}As$ quantum wells, which are example of epitaxial interfaces with small difference in mean inner potential (the non-binding approximation yields ΔV_0=0.4 V) [15]. Because of the small ΔV_0 the layers can be distinguished by inspection only in the zone axis orientation (Fig. 8c and d) where most of the contrast is due to dynamical diffraction. Averaged phase profiles from identical specimen areas yield a phase difference of $\approx\pi/2$ between the GaAs and the $Al_{0.3}Ga_{0.7}As$ layers in the zone axis orientation, while the difference is $<\pi/10$ for the systematic raw orientation.

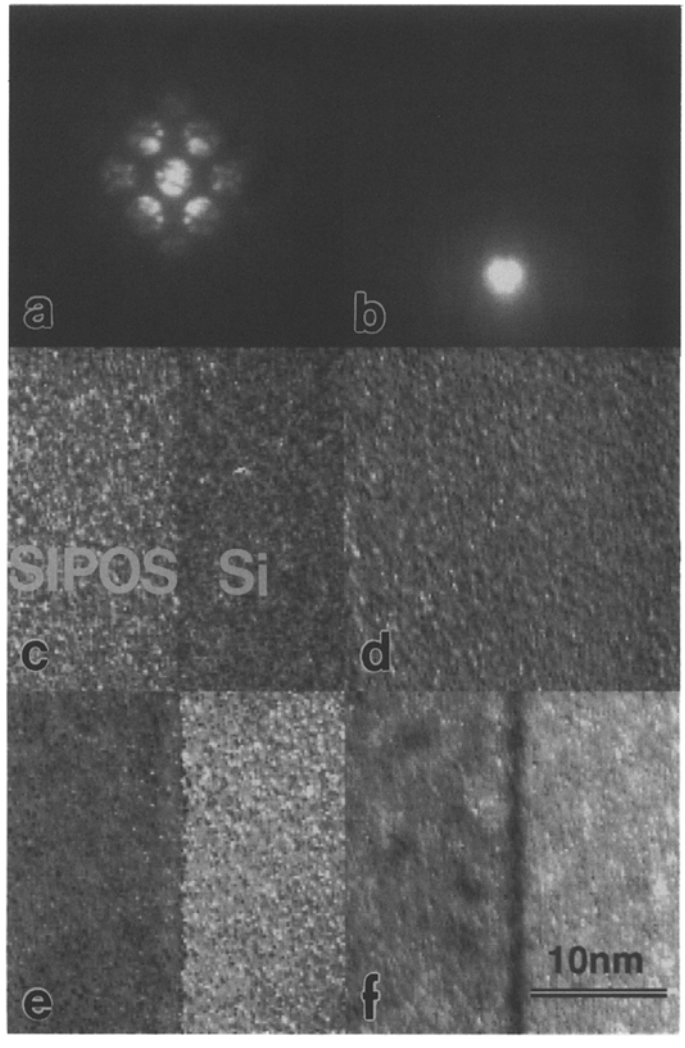

Fig. 9. Interface between Si(111) and polycrystalline SIPOS at [0, −1, 1] zone axis (a, c, e) and at (111) systematic row (b, d,f) orientation. The amplitude (c) and phase (d) images at the zone axis orientation show an abrupt interface, while in the systematic row orientation the amplitude shows no contrast (d) and the phase image (f) reveals a 1 nm wide region with less phase advancement (f).

The tilting options have the same restrictions when amorphous and/or polycrystalline films are grown on single crystal substrates with a surface parallel to a crystallographic plane. The Si/SIPOS interface shown in Fig. 9 is an example of such case. SIPOS is a polycrystalline semi-insulating oxygen doped silicon. The SIPOS film is a reference for the holograms (as in Fig. 2d). Tilting parallel to the interface changes the contrast in the phase and amplitude images drastically. The amplitude contrast vanishes in the systematic raw orientation (Fig. 9d), while the phase image from the same hologram displays a phase retardation at the interface (see dark band in Fig. 9f).

4.2.3 Effects of Defocus. The effects of defocus on medium resolution holography is demonstrated in Fig. 10. An MBE grown $NiSi_2$/Si(111) interface is used. The cross-sectioned specimen is tilted to the systematic {111} row orientation. The hologram for the middle raw of images was recorded at approximate Gaussian defocus, while the images above and below correspond to an overfocus and underfocus of 1 μm respectively. The most pronounced effect of defocus are the Fresnel fringes at the vacuum/$NiSi_2$ and the $NiSi_2$/Si interfaces. The profiles in Fig. 10 show that the Fresnel fringes are more pronounced in the amplitude compared to the phase image. The most

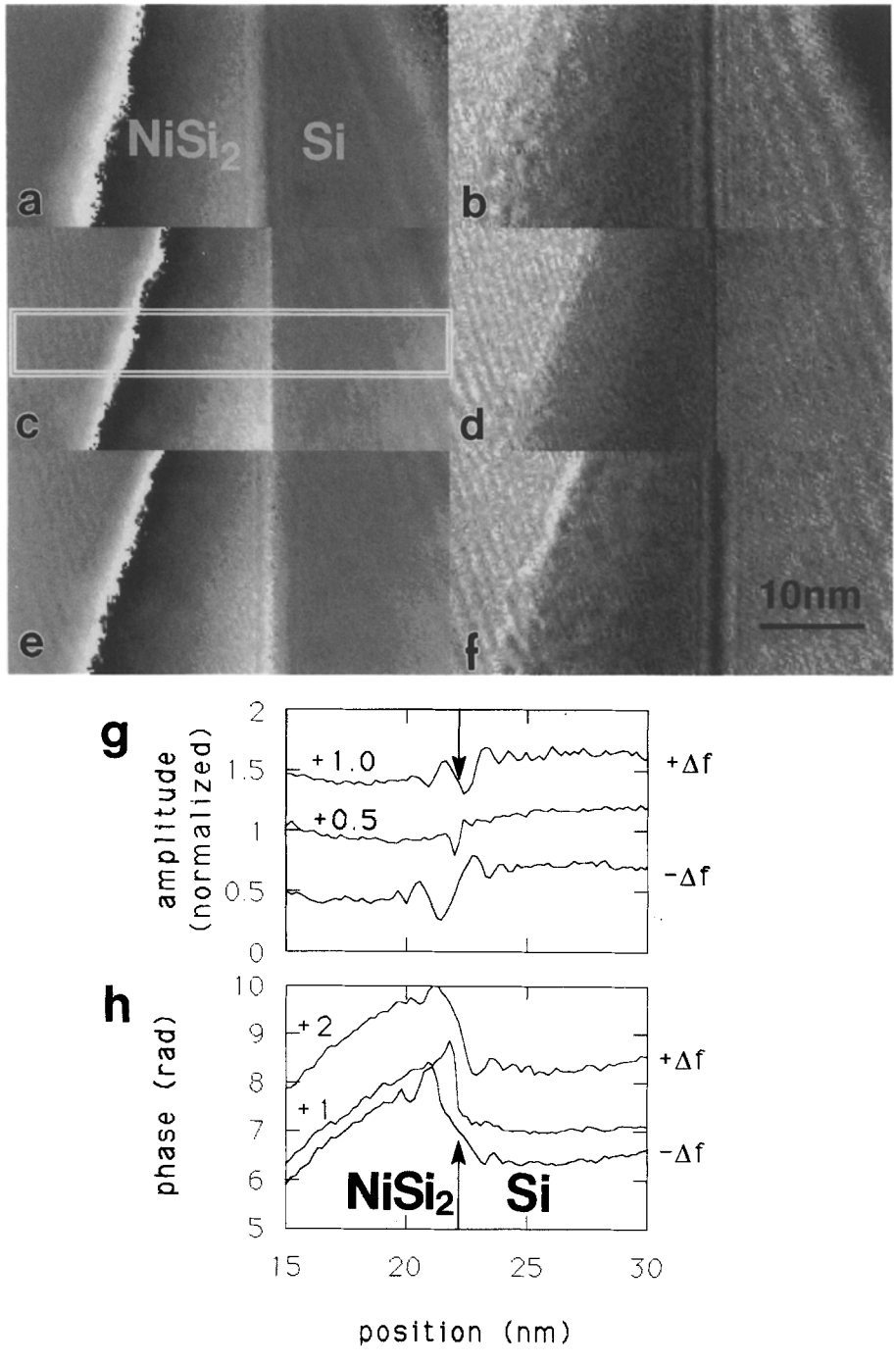

Fig. 10. Effects of defocus on phase (a, c, e) and amplitude (b, d, f) images from $NiSi_2$/Si(111) interface tilted to systematic (111) row orientation: (a, b) over focus of $\Delta f = +1$ μm; (c, d) Gaussian focus $\Delta f \approx 0$; (e, f) under focus of $\Delta f = -1$ μm. The profiles in (g) and (h) are extracted from boxed region and averaged in the direction parallel to the interface. Fresenel fringes at the interface are more pronounced in defocused amplitude images.

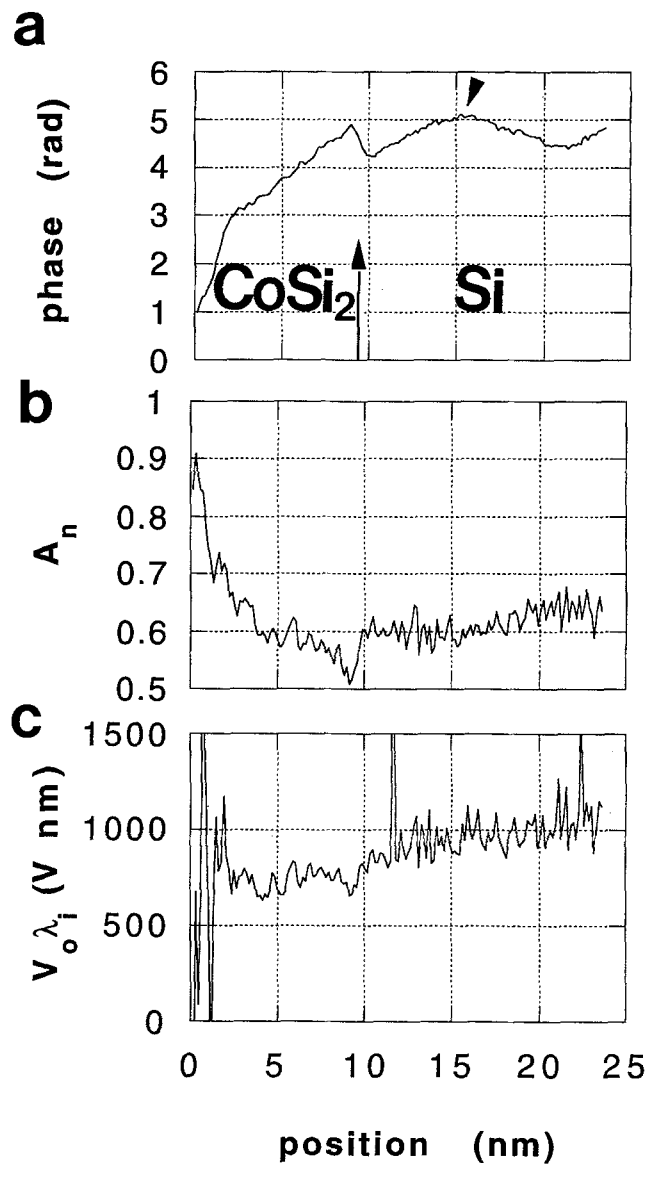

Fig. 11. Elimination of thickness dependence by combining phase and normalized amplitude using Eq. 8. Example shows phase (a) and amplitude (b) profiles from $CoSi_2$/Si interface (as in Fig. 7b and d) from region with large phase advance in Si region. Ratio profile in (c) maps product of mean inner potential (V_0) and mean free path for inelastic scattering (λ_i) across the interface. It indicates that arrowed hump in Si phase profile is due to thickness variation, rather than to composition variation.

pronounced feature in the phase profile is the large jump of $\sim\pi/2$ at the interface which becomes less abrupt when the hologram is recorded with defocus.

4.2.4 Compositional Interface Images: Combination of Amplitude and Phase Information. The amplitude images, reconstructed from off-axis electron holograms, are energy filtered. In holograms where vacuum is used as a reference, the amplitude image can be normalized ($A_n = A_o A_r / A_r^2$) to yield unity in vacuum. In the absence of strong dynamical diffraction effects, the normalized amplitude is an exponentially decreasing function with specimen thickness (t) [24]:

$$A_n = \exp\left(-\frac{t}{2\lambda_i}\right) \tag{7}$$

where λ_i is the mean free path for inelastic scattering.

The thickness dependence of the amplitude and phase images is usually an impediment in studies of interfaces, because most cross sectional specimen have unknown and/or irregular thickness. We have shown recently [13] that the thickness dependence can be eliminated by combining the phase and amplitude image reconstructed from the same hologram. These two images are in perfect registry with each other and both are function of the specimen thickness. By dividing the phase image with a logarithm of the amplitude image (see Eqs. 5a and 7) we obtain a composition image that is independent of thickness:

$$\frac{\phi}{-\frac{4\pi e}{\lambda E}\frac{E_0+E}{2E_0+E}\ln A_n} = V_0\lambda_i \qquad (8)$$

In the kinematical approximation this image is the product of the mean inner potential and the mean free path for inelastic scattering.

Figure 11 illustrates this method using a hologram from a $CoSi_2$/Si interface. This sample was tilted to a systematic row orientation as in Fig. 7c and d. The phase profile in Fig. 11a shows a hump in the Si substrate, which has a corresponding but less pronounced dip in the normalized amplitude profile in Fig. 11b. The profile in Fig. 11c shows the ratio calculated from Eq. 8. Although the noise of the amplitude image is further amplified in the division procedure, the compositional profile shows that the hump in the phase image was due to thickness variation in Si and not to composition variation. It also demonstrates that difference in mean free paths is larger than the difference in mean inner potential between $CoSi_2$ and Si, yielding two distinct values of the $V_0\lambda_i$ product in the two materials.

5 Conclusions

The field of interface holography is very new. It is in the stage of development of experimental and theoretical methods. The motivation is kept strong by the prospects for higher spatial resolution, energy filtering, and sensitivity to electric and magnetic fields. Holography is also sensitive to topography, structure and composition.

The first applications of electron holography have been to homogeneous interfaces, such as *p-n* junctions, and domain walls in magnetic and ferroelectric materials. Equiphase lines in the reconstructed phase images map the equipotential lines of electrostatic fields, and the lines of induction of magnetic fields.

The studies of heterogeneous interfaces are more recent. The first applications to amorphous/polycrystalline multilayers have shown that phase images map the mean inner potential *and* the specimen thickness. For crystalline interfaces the dynamical diffraction contributions to the phase are dominant in zone axis orientations, and strong in systematic row orientations. Dynamical calculations, which include the mean inner potential, will need to be developed to interpret the quantitative phase images from crystalline hetero-interfaces.

The amplitude and phase images reconstructed from holograms are energy filtered, i.e. only the elastically scattered electrons contribute to these images. The two images can be combined to distinguish between topography and composition information, which is particularly important for study of hetero-interfaces with unknown specimen thickness.

In conclusion, the possibilities of electron holography for study of interfaces in solids are yet to be explored in full. The first results show promising future.

Acknowledgments

The author is grateful to W.J. de Ruijter, M.R. McCartney, D.J. Smith and J.K. Weiss for the many discussions and collaboration on various parts of the research which was reviewed in this paper. The interfaces studied were courtesy of R. Tung, J. Marakas and R. Carpenter. The research was conducted at the Center for High Resolution Electron Microscopy at Arizona State University, supported by the National Science Foundation under grant DMR91-15680.

References

1. D. Gabor, Nature **161**, 777 (1948).
2. A. Tonomura, Advances in Physics **41**, 59 (1992).
3. J.M. Cowley, Ultramicroscopy **41**, 335 (1992).
4. **Note**: In the broader sense of the word, the high resolution electron micrographs (HREM) from crystalline interfaces, and the Fresnel fringes from interfaces, can be treated as in-line holograms since both contain phase information due to the interference between transmitted and scattered electrons. However, the amplitude and phase of the image wave can not be reconstructed from one such image.
5. R. Lauer, in *Proc. 10th Int. Congr. Electron Microscopy*, Vol. 1 (Hamburg, 1982), pp. 427–428.
6. K.-J. Hanszen, J. Phys. D: Appl. Phys. **19**, 373 (1986).
7. G. Möllenstedt and H. Dücker, Z. Physik. **145**, 377 (1956).
8. M. Vanzi, Optik **58**, 103 (1981).

9. H. Lichte, Electron Image Plane Off-Axis Holography of Atomic Structures, in: *Advances in Optical and Electron Microscopy*, Vol. 12 (Academic Press, London, 1991), p. 25.
10. W.J. de Ruijter and J.K. Weiss, Ultramicroscopy **50**, 269 (1993).
11. J.K. Weiss, W.J. de Ruijter, M. Gajdardziska-Josifovska, D.J. Smith, E. Voelkl, and E.H. Lichte, in *Proc. 49th Annual EMSA Meeting*, edited by G.W. Bailey, (San Francisco Press, San Francisco, 1991), pp. 674–675.
12. J.K. Weiss, W.J. de Ruijter, M. Gajdardziska-Josifovska, M.R. McCartney, and D.J. Smith, Ultramicroscopy **50**, 310 (1993).
13. M. Gajdardziska-Josifovska and M.R. McCartney, Ultramicroscopy **53**, 291 (1994).
14. G.L. Waytena, J. Hren, and P. Rez, J. Appl. Phys. **73**, 1750 (1993).
15. M. Gajdardziska-Josifovska, in *Proc. 51st Annual MSA Meeting*, edited by G.W. Bailey and C.L. Rieder (San Francisco Press, San Francisco, 1993), p. 1090.
16. J.K. Weiss, M. Gajdardziska-Josifovska, M.R. McCartney, and D.J. Smith, in *Proc 50th Ann. MSA Meeting*, edited by G.W. Bailey, G. Bentley, and J.A. Small (San Francisco Press, San Francisco, 1992), p. 244.
17. P.G. Merli, G.F. Missiroli, and G. Pozzi, J. Microscopie **21**, 11 (1974).
18. S. Frabboni, G. Matteucci, and G. Pozzi, Phys. Rev. Lett. **55**, 2196 (1985).
19. D.C. Joy, X. Zhang, A. Mohan, and B. Cunningham, in *Proc. 51st Annual MSA Meeting*, edited by G.W. Bailey and C.L. Rieder, (San Francisco Press, San Francisco, 1993), p. 1094.
20. S. Miyake, K. Fujiwara, and K. Suzuki, J. Phys. Soc. Jpn. **18**, 223 (1963).
21. X. Zhang, T. Hashimito, and D.C. Joy, Appl. Phys. Lett. **60**, 784 (1992).
22. V.P. Dravid, V. Ravikumar, and R. Plass, in *Proc. 51st Annual MSA Meeting*, edited by G.W. Bailey and C.L. Rieder (San Francisco Press, San Francisco, 1993), p. 1088.
23. M. Gajdardziska-Josifovska, MSA Bulletin **24**, 507 (1994).
24. M.R. McCartney and M. Gajdardziska-Josifovska, Ultramicroscopy **53**, 283 (1994).
25. H. Lichte, Ultramicroscopy **20**, 293 (1986).
26. A. Harscher, F. Lenz, and H. Lichte, *X European Congress on Electron Microscopy*, (Granada, Spain, 1992), pp. 35–36.
27. Z.L. Wang, Ultramicroscopy **52**, 504 (1993).
28. M. Gajdardziska-Josifovska, M.R. McCartney, W.J. de Ruijter, D.J. Smith, J.K. Weiss, and J.M. Zuo, Ultramicroscopy **50**, 285 (1993).
29. E. Völkl and H. Lichte, Ultramicroscopy **32**, 177 (1990).
30. L. Reimer, in *Tranmsission Electron Microscopy*, Springer, Berlin, (1989).
31. H. Lichte, P. Kessler, F. Lenz, and W.-D. Rau, Ultramicroscopy **52**, 575 (1993).
32. T. Kawasaki and A. Tonomura, Phys Rev. Lett. **69**, 293 (1992).
33. H. Lichte, E. Völkl, and K. Scheerschmidt, Ultramicroscopy **47**, 231 (1992).
34. H. Lichte, Ultramicroscopy **38**, 13 (1991).
35. M. Gajdardziska-Josifovska, J.K. Weiss, and J.M. Cowley, Ultramicroscopy, in press.
36. A.K. Petford-Long, M.B. Stearns, C.-H. Chang, S.R. Nutt, D.G. Stearns, N.M. Ceglio, and A.M. Hawryluk, J. Appl. Phys. **61**, 1422 (1987).
37. X. Zhang, T. Hashimoto, and D.C. Joy, Appl. Phys. Lett. **60**, 784 (1992).